ELSEVIER

Contents lists available at ScienceDirect

Geomechanics for Energy and the Environment

journal homepage: www.elsevier.com/locate/gete



A study on the hydraulic aperture of microannuli at the casing-cement interface using a large-scale laboratory setup



Al Moghadam*, Koen Castelein, Jan ter Heege, Bogdan Orlic

TNO Energy Transition, The Netherlands

ARTICLE INFO

Article history: Received 7 April 2021 Received in revised form 16 July 2021 Accepted 16 July 2021 Available online 28 July 2021

Editors-in-Chief: Professor Lyesse Laloui and Professor Tomasz Hueckel

Keywords: Well leakage Microannuli Hydraulic aperture Mechanical aperture Residual aperture

ABSTRACT

Presence of microannuli at the cement interfaces in wellbores could provide a path for fluid leakage. In this study, we combined experimental analysis and numerical modelling to assess microannuli development at casing–cement interfaces. Lab experiments were conducted using two-metre long samples consisting of a 7" casing cemented inside a rock analogue (stiffer, stronger cement) encased with a steel outer shell. Hydraulic aperture of the microannuli was calculated by measuring water flow through the casing–cement interface at various casing pressures and after axial displacements. The results show that once a microannulus forms, it remains open at internal casing pressures as high as 40 MPa. The measured hydraulic apertures were in the range of tens of microns, with residual apertures in the range of 15 to 30 μm . Axial displacement of the casing did not lead to a significant change in the hydraulic apertures. A numerical model was created with a comparable geometry to the experiments, and used to calculate the mechanical apertures of the microannuli. A relationship is proposed to link the mechanical apertures from the numerical models to the hydraulic apertures measured in large-scale experiments. The findings enable the operators and regulators to improve safe well operation practices by forecasting the conditions that lead to possible loss of zonal isolation and the associated well leakage rates.

© 2021 The Author(s). Published by Elsevier Ltd. This is an open access article under the CC BY-NC-ND license (http://creativecommons.org/licenses/by-nc-nd/4.0/).

1. Introduction

Wellbores are commonly used as an artificial pathway to produce or inject fluids in applications such as water, gas, and oil production, or waste fluid, hydrogen, and CO₂ storage. Drilling a well through various strata introduces a risk of fluid communication between different formations and upward migration of substances. This can ultimately lead to the contamination of the subsurface water sources or leakage of fluids to surface. ^{1,2} To mitigate the risk of leaks, well designs usually consist of several cemented steel casings placed in the wellbore at several depths, with multiple casings that partly overlap at shallow depths. The casings are cemented in place by pumping cement slurry through the casing which subsequently flows through the annular space between overlapping casings or between the casing and rock formations. Once the cement is cured and set, it acts as a barrier to flow in the annulus, ensuring zonal isolation of the well.

It is critical to ensure the integrity of the annular cement over the entire operational lifetime of the well, as well as after decommissioning of the well. Best practice approaches include ensuring appropriate type of cement and cementation procedures are used given the expected downhole conditions of pressure, temperature, and the chemical environment.³ Subsequent well operations can also damage the cement by causing expansion or contraction of the casing resulting from changes in temperature or pressure during injection or production.⁴ Well integrity issues caused by well operations is of particular interest for energy storage, geothermal energy, and carbon sequestration projects, particularly when re-using old oil and gas wells.⁵⁻⁹ A poorly placed and damaged cement sheath can create a permeable zone around the casing that allows fluids to move upwards or downwards. Cement damage may also expose the casing to chemically reactive downhole fluids, which may promote casing corrosion and degradation. 10 Mitigation of well leakage is generally difficult and expensive. Therefore, it is critical to assess the well conditions that can lead to cement damage and the resulting rate of fluid leakage upfront. If incorporated in well design, such assessments can help de-risking well operations based on project-specific well integrity analysis.

There are several types of cement failure that could occur under downhole conditions. High pressures inside the casing can change the tangential stress in cement from compression to tensile, leading to radial cracks.¹¹ Cement can also fail in shear at high deviatoric stresses^{12,13} or due to heating or cooling of the well.^{14,15} Differential axial displacement between formation, casing, and cement (e.g. due to shrinkage) can lead to disking (flat

^{*} Corresponding author. E-mail address: al.moghadam@tno.nl (A. Moghadam).

horizontal cracks across the cement). Additionally, the cement sheath can debond from the casing or the formation, leading to the creation of microannuli. A microannulus can be formed by casing contraction due to cold fluid injection, such as CO₂, and by a drop in casing pressure. Cement hydration and high formation pressure have also been proposed as causes of microannulus formation. Significant significant control of the companion of the co

There is a long history of model development to predict failure in cement sheaths. Thiercelin et al.²⁰ developed an analytical model to investigate cement failure in wellbores. Bosma et al.²¹ presented a finite element model to study various loading scenarios. They also investigated the impact of different initial stress assumptions on the cement sheath integrity calculations. Their results indicated that cement's elastic properties are important design parameters to reduce the risk of cement failure under in-situ conditions. Gray et al.²² provided a review of the finite element models in the literature, and emphasized the need for modelling the entire load history of the well. Bois et al.4 proposed the use of a mechanistic model that simulates the hydration process of cement. Their model was used to predict various types of cement failure and the results were verified using lab experiments. Lavrov²³ conducted a numerical study to investigate the conditions that could lead to the debonding of casing and cement. They concluded that the impact of thermal stresses can be reduced by adjusting the stiffness of the cement with respect to the stiffness of the formation. Orlic et al.9 investigated the impact of well history on the formation of the microannulus. Roy et al. 17 studied the impact of thermal stress on cement integrity using numerical simulations and concluded that presence of sufficient in-situ stresses can mitigate the impact of the microannulus. Frash and Carey²⁴ developed analytical and numerical schemes to study the impact of reservoir uplift on the shear integrity of the cement sheath. Zhang and Eckert²⁵ incorporated the impact of cement pore pressure and stiffness development in a staged finite element model. Numerical models are important tools in studying the annular cement integrity. However, models should be verified using laboratory experiments or well logs to ensure their accuracy in predicting loss of cement integrity.

Goodwin and Crook²⁶ conducted laboratory experiments on the integrity of cement placed in the annular area between two casings. They measured the evolution of annular permeability under various pressure cycles. Jackson and Murphey²⁷ used a similar setup to test different pressure cycles and well configurations. These experiments indicated that at high inner casing pressures, no permeability was observed. However, as the pressure was dropped significant permeability was created in the annular region. This indicated plastic deformation at high casing pressures which lead to debonding as pressure is dropped. 1 Boukhelifa et al.²⁸ used an apparatus capable of mechanically expanding and contracting the casing to study the impact of casing deformation on the integrity of annular cement. They tested various cement formulations and concluded that the use of more flexible cements can prevent debonding. Therond et al. 29 used a large-scale setup to study the impact of pressure and temperature cycles on cement integrity. A postmortem analysis of their samples indicated the presence of radial cracks, disking, and microannuli. They concluded that the formation of microannuli has the biggest impact on the annular permeability. Radial cracks showed significantly lower permeability in their experiments. De Andrade et al. 30 developed an experimental setup to investigate cement failure under various loading conditions using X-ray computed tomography. The new experimental setup allowed for 3D visualization of radial cracks and microannuli.¹¹ Stormont et al.31 conducted a comprehensive set of tests on microannulus aperture under various confining stress and casing pressures. The measured apertures in their work ranged between 0.6 μm (for the intact cement) and 60 μm , for the majority of the tests. Their results show that microannuli could allow high permeability channels to form. Although casing pressure can close the microannulus to some degree, a residual permeability always seems to exist. Welch et al. 32 used a triaxial direct shear setup to measure the cohesion and friction angle of the cementsteel interface. Their results showed little change in the interface permeability due to shear displacement.

The permeability of the damaged cement is a critical parameter, as it determines the rate of fluid migration along the wellbore. A cement sheath with high permeability induced by fractures or debonding could ultimately lead to contamination of shallow water sources if fluid pathways connect over large parts of the well. Also, lack of zonal isolation over large well sections can lead to emission of greenhouse gases such as methane into the atmosphere, and or can jeopardize the seal quality of CO₂ storage sites. Formation of continuous microannuli due to debonding of the casing–cement interface could lead to permeable pathways between casing and cement. 29,31

Differential sliding between the casing and the cement can lead to shear displacement along the casing–cement interface. This could also lead to a change in the microannulus aperture, which is not as clearly understood as debonding. Hydromechanical properties of the microannulus are needed to correctly assess the severity of leakage in the annular region. These parameters are critical inputs in models to estimate the aperture and permeability evolution of microannuli over the well's history. While there are studies in the literature that measure hydraulic aperture change with casing pressure³¹ and shear displacement,³² they are conducted on small samples that fit in a typical triaxial cell. Large-scale tests that more closely represent the wellbore geometry are still scarce.

In this study, we used lab experiments and numerical modelling to assess microannuli development at casing-cement interfaces. We conducted flow experiments on two-metre long samples that consist of a 7" casing and annular cement. Hydraulic aperture of the microannuli was calculated from the flow data at various casing pressures, and after axially displacing the casing through the annular cement. We developed a numerical model to calculate the mechanical aperture of the microannulus under conditions similar to the laboratory experiments. Using the experimental and modelling results, we propose a new relationship between the mechanical and hydraulic apertures for casing-cement microannuli. We compared the experimental results to surface leakage measurements at abandoned oil and gas well sites, collected from several studies in the literature, to evaluate the apertures and associated leakage rates of the microannuli against actual field measurements.

The results provide estimates of the hydraulic properties of microannuli in well systems at realistic spatial scales, which are critical for reliable modelling of well leakage. In addition, the experimental results on the large-scale samples provide benchmark data for hydraulic aperture and leakage that can be used to verify numerical models and to better understand the mechanisms controlling the opening and closure of microannuli. This work attempts to fill the existing gaps between the numerical modelling, laboratory experiments, and field-scale measurements of fluid leakage in wells. It enables more accurately forecasts of the conditions for loss of zonal isolation and quantifies possible well leakage rates for a wide range of geological and operational conditions.

2. Approach

2.1. Microannulus aperture

In this study, a microannulus is treated as a distinct fracture with a mean aperture. Conventional cubic law for fluid flow

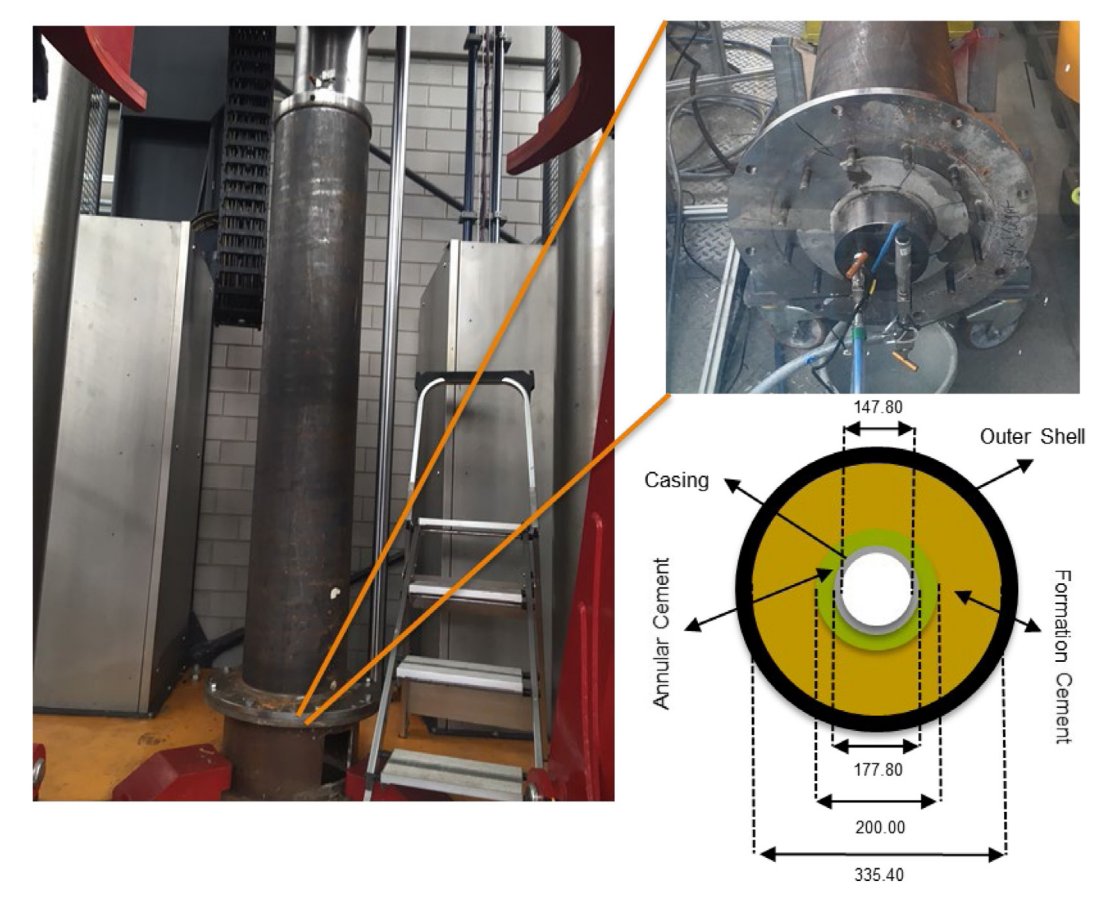


Fig. 1. A schematic of the samples in this study next to pictures of an actual sample. Green represents annular cement, and yellow indicates the formation analogue. The dimensions in the figure are in mm. The picture on the left shows the outer shell but presents the full length of the sample. The picture on the right shows the bottom face of the sample including the casing, annular cement, formation cement, and the outer shell.

along fractures can then be used to relate the aperture of the microannulus to permeability and flow rate.³⁵ Eq. (1) shows the relationship between the flow rate and the aperture of the microannulus for an incompressible fluid.³⁶

$$Q = -\frac{e_h^3}{12} x_a \frac{\Delta P}{\mu L} \tag{1}$$

Q in Eq. (1) is the flow rate, e_h is the hydraulic aperture of the microannulus, x_a is the circumference of the microannulus, ΔP is the pressure difference across the microannulus, μ and L are fluid viscosity and length of the annulus, respectively.

Geomechanical models are generally capable of calculating the aperture change due to a change in loading conditions. 9,18,37 However, these models calculate the mechanical aperture of the microannulus. Hydraulic aperture of the microannulus is required to calculate leakage rates using Eq. (1). Hydraulic aperture of a fracture is typically lower than the mechanical aperture due to the roughness of the fracture faces and the tortuosity of flow paths.³⁸ Several studies have proposed correlations to calculate the hydraulic aperture of a single fracture using the mechanical aperture and some form of roughness coefficients.³⁹⁻⁴¹ However, the relationship between the hydraulic and mechanical apertures of cement microannuli is largely unknown. Understanding this relationship is paramount in filling the gap between predictions of the geomechanical models and fluid leakage calculations. A new relationship between the hydraulic and mechanical aperture of microannuli is proposed in the discussion section.

2.2. Experimental design

2.2.1. Sample and setup description

The samples in this work consisted of a two-metre long steel shell with an inner diameter of 355.4 mm (14"). The shell was ordered from a commercial company and included a cement (Gouda Vuurvast, uniaxial compressive strength of 37 MPa) already casted inside with a 200 mm hole to fit a smaller casing. The cement in the shell was intended to simulate the formation. The formation cement was stiffer and stronger than the annular cement used in this study. A standard casing with an outer diameter of 177.8 mm (7") was placed and centred in the hole of the formation cement. Water was injected into the casing to raise the inner pressure to 20 MPa. A cement slurry was created by mixing class G Portland cement with water with a ratio of 0.4 w/c. The cement slurry was mixed at 7000 rpm until it was smooth.⁴² The slurry was then pumped into the annular space between the casing and the formation cement, using a membrane pump. The cement was cured for approximately seven days at 0.3 MPa pressure and room temperature. The curing pressure was applied using a nitrogen cushion at the top of the cement. During the curing period, the inner casing pressure was maintained at 20 MPa. Subsequently, the casing pressure was dropped to zero to create a microannulus at the casing-cement interface.

To conduct the experiments, the samples were placed vertically in a load-frame capable of exerting an axial load up to 140 metric tons on the casing. In addition, the setup was capable of controlling the fluid pressure inside the casing. To measure the hydraulic aperture, tap water was pumped through the bottom of the annulus at a constant rate between 7.5 to 150 ml/min using a

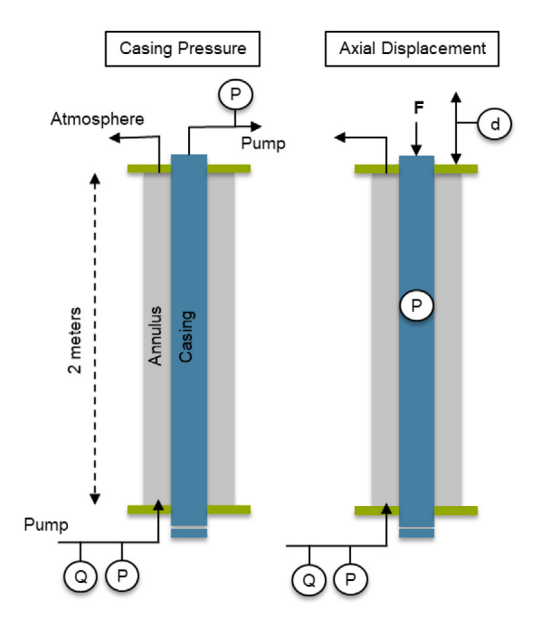


Fig. 2. A schematic of tests conducted in this work. "P" indicates pressure measurement, "Q" indicates flow rate, "F" indicates force, and "d" indicates displacement.

H3 metring pump until the inlet pressure stabilized (between 0.2) to 5 MPa, accurate to $\pm 0.1\%$). The top of the annulus was open to the atmosphere. The flow rate was measured at the pump and using an automatic scale at the downstream, with an accuracy of $\pm 0.25\%$. Hydraulic aperture was calculated using Eq. (1) using the measured flow rate and upstream pressure. The viscosity of water was assumed to be 0.9 cp. Each measurement of the hydraulic aperture took 15 to 30 min until the flow stabilized. Fig. 1 shows details of the setup and samples. In this study, two samples were created to investigate the impact of casing pressure change, and axial displacement of the casing on the hydraulic aperture of the microannulus. All experiments have been conducted at the Rijswijk Centre for Sustainable Geoenergy (RCSG) in the Netherlands. A brief description of the experimental setup and the preliminary results are also reported by Moghadam et al.⁴³.

2.2.2. Casing pressure experiments

In the first set of experiments, we investigated the impact of casing pressure (ballooning) on the hydraulic aperture of the microannulus (Fig. 2). The sample was prepared as described in the previous section. A microannulus was formed by dropping the casing pressure from an initial value of 20 MPa during curing, to zero (gauge pressure). Water flow was then established at a constant rate in the annular region to measure the hydraulic aperture, using Eq. (1). For each measurement, we recorded the flow rate and the upstream annular pressure after the flow was stabilized (no pressure change for 15 to 30 min). The inner casing pressure was then raised, and another flow test was conducted to quantify the impact of casing pressure on the aperture of the microannulus. The casing pressure was gradually increased to 40 MPa with hydraulic aperture being measured at each step. The casing pressure was then dropped in several steps back to the atmospheric pressure, while measuring the hydraulic aperture during the unloading stage. The casing pressure was cycled three times. The annular flow rate was changed for each cycle to investigate its impact on the hydraulic aperture.

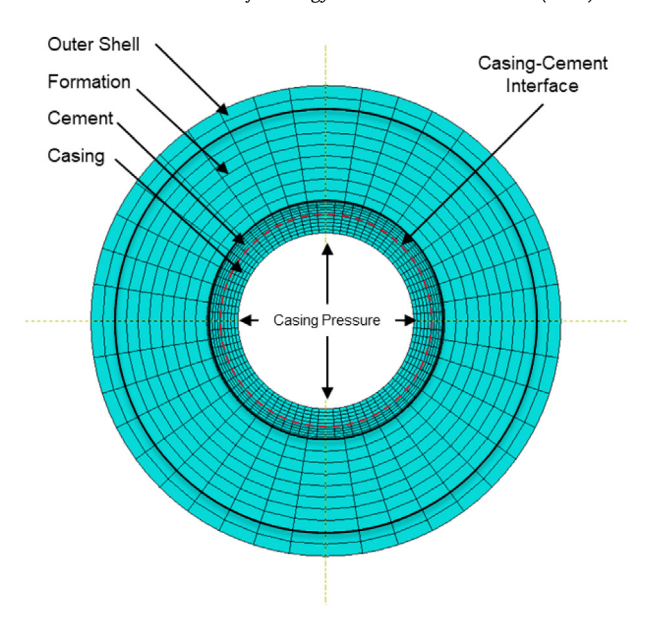


Fig. 3. The geometry of the finite element model.

2.2.3. Axial displacement experiments

The second sample in this work was used to study the impact of axial movement of casing on the microannulus (Fig. 2). After the sample preparation and the creation of a microannulus, the casing pressure was set back to 20 MPa and the hydraulic aperture was measured at two different flow rates (i.e. upstream pressures). An axial load was then applied at the top of the casing using a load frame, while maintaining a 20 MPa pressure inside the casing. The load increased gradually until the casing was displaced uncontrollably, indicating shear failure at the casingcement interface. The casing was axially loaded again to measure the hydraulic aperture after another displacement. The casing was displaced 7 times in total for this experiment. Fig. 2 illustrates a schematic of the setup for both experiments.

2.2.4. Test overview

Table 1 summarizes all the tests conducted in this work. Each test includes several hydraulic aperture measurements. The experiments will be referred to by their test ID, in the rest of the paper. Table 1 also provides a short description for each test and indicates the figure numbers that display the main data.

2.3. Numerical modelling

The commercial finite element package Abaqus⁴⁴ was used to model the microannulus aperture change for the casing pressure experiments. The geometry of the sample was represented by a 2D plane strain model as shown in Fig. 3.

Standard steel properties were used for the outer shell and the casing. The cement properties were taken from the laboratory experiments on class G Portland cement in the literature⁴⁵. The properties of the formation cement were supplied by the manufacturer.

Table 2 summarizes the material properties used in the numerical model.

We modelled the interfaces between the casing, cement, formation, and the outer shell using the surface-to-surface contact discretization method (Abaqus/Standard User's Manual, 2019). This formulation allowed us to set the debonding status and the initial aperture of the interfaces, in order to calculate the mechanical aperture of the microannulus with a change in casing pressure. A cohesive contact model was used to simulate

Table 1Summary of the experiments conducted in this work.

Test ID	Sample number	Figure number	Test name	Test description
CP-7.5-L	1	Fig. 4	Casing pressure	Casing pressure increased from 0 to 35 MPa, constant flow rate of 7.5 ml/min
CP-7.5-U	1	Fig. 4	Casing pressure	Casing pressure decreased from 35 to 0 MPa, constant flow rate of 7.5 ml/min
CP-60-L	1	Fig. 4	Casing pressure	Casing pressure increased from 0 to 40 MPa, constant flow rate of 60 ml/min
CP-60-U	1	Fig. 4	Casing pressure	Casing pressure decreased from 40 to 0 MPa, constant flow rate of 60 ml/min
CP-60-LR	1	Fig. 4	Casing pressure	Repeat of CP-60-L test
CP-150-L	1	Fig. 4	Casing pressure	Casing pressure increased from 0 to 40 MPa, constant flow rate of 150 ml/min
CP-150-U	1	Fig. 4	Casing pressure	Casing pressure decreased from 40 to 0 MPa, constant flow rate of 150 ml/min
AD-PS	2	Fig. 6	Axial displacement	Prior to the axial loading of the casing 20 MPa casing pressure, constant flow rates of 60 and 150 ml/min
AD-S1	2	Fig. 6	Axial displacement	Axial displacement of casing through the cement, displacement 1 20 MPa casing pressure, constant flow rates of 60 and 150 ml/min
AD-S2	2	Fig. 6	Axial displacement	Axial displacement of casing through the cement, displacement 2 20 MPa casing pressure, constant flow rates of 60 and 150 ml/min
AD-S3	2	Fig. 6	Axial displacement	Axial displacement of casing through the cement, displacement 3 20 MPa casing pressure, constant flow rates of 60 and 150 ml/min
AD-S7	2	Fig. 6	Axial displacement	Axial displacement of casing through the cement, displacement 7 20 MPa casing pressure, constant flow rates of 60 and 150 ml/min

Table 2Summary of the material properties used in the numerical model.

Parameter	Unit	Casing and outer shell	Formation	Cement	Contacts
Young's modulus	GPa	200	15	8	_
Poisson's ratio	-	0.26	0.2	0.2	-
Cohesion	MPa	_	10	10	_
Friction angle	0	_	30	20	_
Casing-cement bond strength	kPa	-	-	-	500

the initial bond between the cement and the casing. Once the tensile stresses at the contact exceeded the bond strength, the cohesive bond was eliminated, and the contact surfaces were free to separate. When appropriate, fluid pressure was applied at the microannulus surfaces after debonding. A von Mises failure criterion was used for the casing and the outer shell, while Mohr–Coulomb failure criterion was used for the cement and the rock formation.

The simulations followed a similar stress path as the experiments. Initially, the inner casing pressure was set to 20 MPa to mimic the pressure during the cement curing stage in the experiments. The annular space between the casing and the formation analog was set to be empty. The cement was then placed in the annular region at an initial stress equal to the curing pressure (300 kPa). The cement was assumed to be fully bonded to the casing and the formation (aperture was set to zero at the interfaces). The casing pressure was then dropped to zero, similar to the procedure followed in all our experiments in order to create the initial microannulus. The casing pressure was raised gradually from 0 to 40 MPa, and fluid pressure was applied to the interface, and the aperture, stresses, and displacements in the model were recorded.

The model was used to calculate the mechanical aperture at all three interfaces, i.e. casing-cement, cement-formation, and formation-shell interfaces. In all the simulations under the laboratory boundary conditions, all changes in aperture occurred at the casing-cement interface. Therefore, in the rest of this paper we refer to the aperture of the casing-cement interface as the aperture of the microannulus.

3. Results

3.1. Impact of casing pressure

The first sample was used to measure the impact of casing pressure on the hydraulic aperture of the microannulus. Fig. 4 shows the change in the hydraulic aperture with respect to casing pressure. The first load cycle, measured at a constant water flow rate of 7.5 ml/min, starts at a hydraulic aperture of 26 μ m at zero casing pressure. This indicates the initial hydraulic aperture of the microannulus that is formed after curing, as the casing pressure is dropped from 20 MPa to zero (at a stabilized upstream pressure of 300 kPa). The aperture decreases as the casing pressure increases, due to casing expansion. The aperture drops to 15 μ m at 35

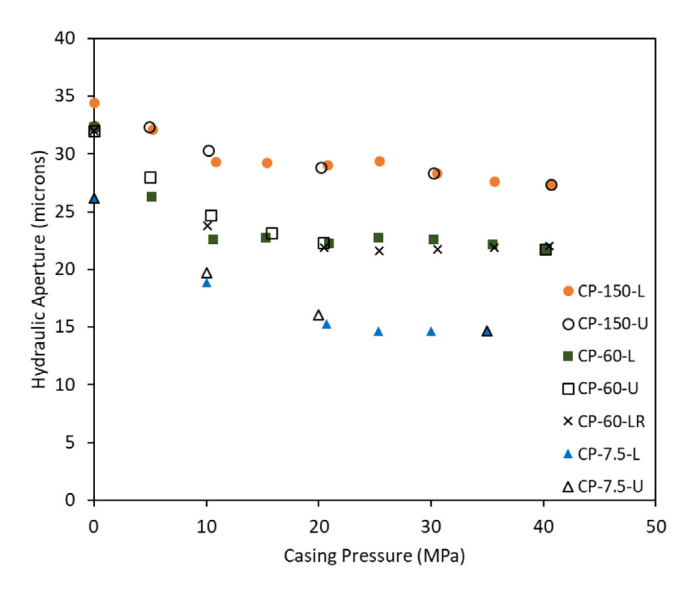


Fig. 4. Hydraulic aperture versus casing pressure for the first sample during three pressure cycles.

MPa during the load cycle. The unloading path in the first cycle indicates similar aperture values as the loading path. During the loading of the second cycle at a flow rate of 60 ml/min, aperture decreases from 32 μ m at 0 MPa to 21 μ m at 40 MPa. As the casing pressure is dropped back to 0, aperture returns to the initial value of 32 µm. The second load cycle was repeated at the same casing pressure and flow rate. The repeated tests show similar results. which indicates acceptable repeatability of the experiments. The hydraulic aperture during the third cycle at 150 ml/min flow rate drops from 35 to 29 μ m, as the casing pressure increases from 0 to 40 MPa. The unloading path follows the same trend. The tests conducted at higher flow rates (i.e. flow pressure) consistently show higher hydraulic apertures. This is due to higher upstream flow pressures needed to maintain a higher flow rate. Table 3 provides a summary of the experimental data for the casing pressure tests.

Fig. 5 shows the numerical results for the mechanical aperture at the casing-cement interface, as the casing pressure is dropped from the initial 20 MPa, during the cement curing, to zero (solid line). According to the results, a microannulus begins to form as the casing pressure reaches 12 MPa. The mechanical aperture of the microannulus increases abruptly to 47 µm when casing pressure is reduced from 12 to 8 MPa. This indicates that the casing-cement interface is fully debonded at 8 MPa. As the casing pressure drops to zero, mechanical aperture increases linearly to 72 μm . When the casing is pressurized again, the microannulus closes linearly with increasing casing pressure, until it is fully closed at 20 MPa. The microannulus remains closed as the pressure further rises to 40 MPa. No failure was observed in the cement elements due to the casing pressurization to 40 MPa. In our flow experiments, water at the inlet of the microannulus is at a pressure between 0.2 to 5 MPa, and at the outlet atmospheric pressure is applied. To account for the impact of water pressure on the microannulus opening, the average water pressure for each test is applied to the cement and casing surfaces at the microannulus. Fig. 5 shows the case for an average water pressure of 2 MPa (average of inlet at 4 MPa and outlet at near zero), as the casing is pressurized. A 2 MPa water pressure expands the microannulus from 72 to 94 µm at zero casing pressure. The microannulus stays open until casing pressure reaches 25 MPa.

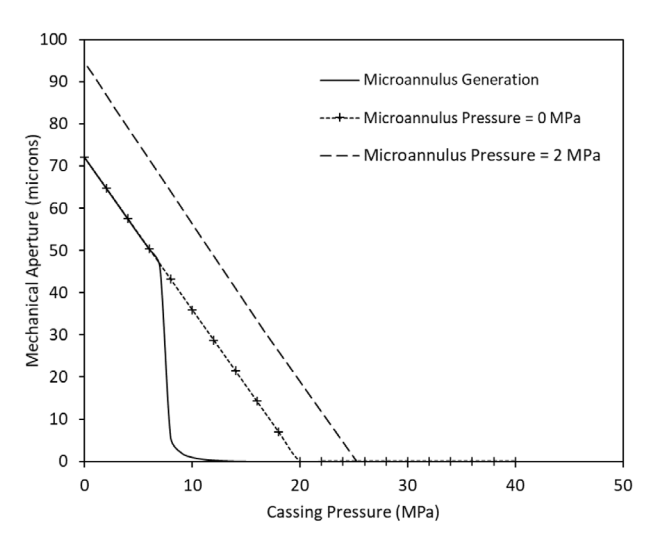


Fig. 5. Mechanical aperture calculated using the numerical model following a similar casing pressure path to the experimental data.

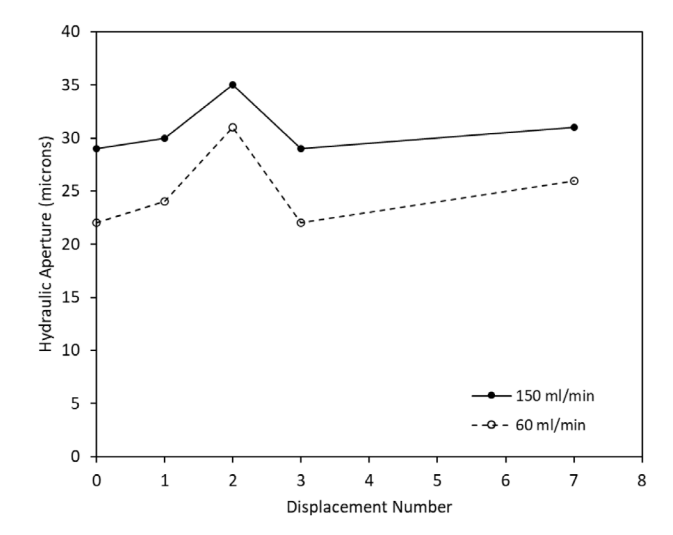


Fig. 6. The change in hydraulic aperture of the microannulus with repetitive axial displacements at 20 MPa casing pressure.

3.2. Impact of axial displacement

In this set of experiments, the casing pressure was held at 20 MPa while the casing was pushed through the annular cement using a load frame. Axial load and casing displacement were recorded. The casing was displaced through the cement seven times in total. Fig. 6 illustrates the hydraulic aperture of the microannulus after repetitive axial casing displacements, at an inner casing pressure of 20 MPa. After each displacement, the hydraulic aperture was measured at flow rates of 60 and 150 ml/min. According to Fig. 6, hydraulic aperture at 60 ml/min flow rate slightly increased from 22 to 30 µm after the first two displacements but dropped back to 22 µm after the third displacement. Hydraulic aperture was only measured again after displacement 7, which showed an increase to 25 μ m. At 150 ml/min flow rate, the hydraulic aperture was consistently higher, ranging between 29 and 35 μm, and following the same trend with the casing displacements. Each casing displacement changed the aperture within a tight range, but no discernible trend was found.

Table 3Summary of the experimental data for the casing pressure (CP) tests.

Test ID	P _{casing} MPa	Flow rate ml/min	P _{upstream} MPa	P _{downstream} MPa	Hydraulic aperture microns
	0	150	2.7	0.1	34.4
	5.2	150	3.35	0.1	32.2
	10.8	150	4.1	0.1	29.3
	15.4	150	4.5	0.1	29.3
CP-150-L	20.8	150	4.6	0.1	29.1
CP-130-L	25.4	150	5	0.1	29.4
	30.5	150	5	0.1	28.3
	35.6	150	5.2	0.1	27.7
	40.7	150	5.3	0.1	27.4
	30.2	150	5	0.1	28.3
	20.2	150	4.7	0.1	28.8
CP-150-U	10.2	150	4.2	0.1	30.3
	4.9	150	3.7	0.1	32.3
	0	150	1.5	0.1	32.3
	5.1	60	2.1	0.1	26.3
	10.6	60	3.2	0.1	22.6
	15.3	60	3.5	0.1	22.8
	20.9	60	3.7	0.1	22.3
CP-60-L	25.3	60	4	0.1	22.7
	30.2	60	4.3	0.1	22.6
	35.5	60	4.3	0.1	22.1
	40.2	60	4.3	0.1	21.7
	20.4	60	3.8	0.1	22.3
	15.8	60	3.6	0.1	23.2
CP-60-U	10.4	60	3.2	0.1	24.7
Cr-00-0	5	60	2.4	0.1	28.0
	0	60	1.7	0.1	32.0
	10.1	60	3	0.1	23.8
	20.5	60	3.9	0.1	21.9
CP-60-LR	25.4	60	4	0.1	21.6
CP-60-LR	30.6	60	4	0.1	21.7
	35.6	60	4	0.1	21.9
	40.5	60	4	0.1	22.0
	20	7.5	1.3	0.1	16.0
CP-7.5-U	10	7.5	0.7	0.1	19.7
C1 7.5 U	0	7.5	0.3	0.1	26.2
	10	7.5	0.8	0.1	18.9
	20.7	7.5 7.5	1.5	0.1	15.3
CP-7.5-L	25.3	7.5 7.5	1.7	0.1	14.7
Cr-/.J-L					
	30	7.5	1.7	0.1	14.7

4. Discussion

4.1. Mechanisms controlling microannulus development

4.1.1. Normal displacement (debonding)

Fig. 5 demonstrates the numerical results of the mechanical aperture opening and closure. As the casing pressure drops, the casing contracts and a microannulus is formed, linearly increasing to a mechanical aperture of 72 μm . The increase in the mechanical aperture is equal to the decrease in the casing outer diameter, largely dependent on the casing material's Young's modulus. Therefore, in the present experiments and model, casing contraction and expansion largely controls the mechanical size of the microannulus. Once the casing is pressurized again, it expands to its original size and completely closes the microannulus (in the mechanical sense), as the casing is expected to be an elastic material under the test conditions.

The behaviour of the hydraulic aperture in the experiments is in some aspects different, as depicted in Fig. 4. As the microannulus is generated by dropping the initial casing pressure to zero, hydraulic aperture increases to a range between 25 and 45 μm , less than the mechanical aperture calculated from the numerical model (94 μm at 2 MPa average flowing water pressure). As the casing is pressurized again, the hydraulic aperture remains open at a residual value between 15 and 30 μm , while the mechanical

aperture fully closes. This behaviour can be attributed to the presence of asperities on the cement's surface that provide residual leakage flow paths even if the microannulus <u>mean</u> mechanical aperture is zero. Therefore, hydraulic aperture values measured in our experiments are not equal to the mechanical apertures predicted by the finite element model. Numerical models assume perfectly smooth surfaces. Therefore, their predictions indicate the mean mechanical aperture. The presence of asperities can lead to a standard deviation from the mean value, which leads to open gaps in the fracture that allow fluid flow, i.e. a residual hydraulic aperture.

In Fig. 4, hydraulic aperture is higher for tests conducted at higher water flow rates. An increase in water rate causes an increase in the average water pressure in the microannulus (Table 3). This leads to further widening of the microannulus. Therefore, the hydraulic aperture is both a function of the casing and microannulus fluid pressure. The impact of fluid pressure is also apparent in the numerical results presented in Fig. 5. During the CP-60-L test, the casing pressure was increased from 0 to 40 MPa. The casing pressure was then dropped to 0 during the CP-60-U test, and re-pressurized again to 40 MPa during CP-60-LR test. The hydraulic aperture was measured at 60 ml/min water flow rate for all three tests. According to Fig. 4, all three tests show similar hydraulic aperture values indicating the reversibility of hydraulic aperture behaviour with casing pressure during three load/unload cycles.

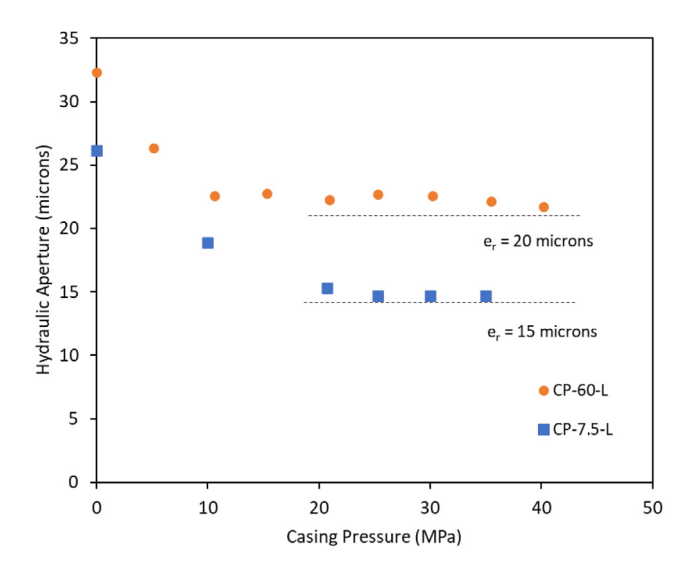


Fig. 7. Residual hydraulic aperture for the CP-60-L and CP-7.5-L experiments.

4.1.2. Shear displacement

Fig. 6 shows the hydraulic aperture of the microannulus after each casing displacement measured at 20 MPa casing pressure and two different flow rates. The hydraulic aperture varies between 29 and 35 μm for 150 ml/min flow rate and between 22 and 30 µm at 60 ml/min flow rate. The increase in hydraulic aperture with flow rate is indicative of the impact of microannulus pressure. The measurements at each flow rate follow the same trend. However, the hydraulic aperture does not show a trend with the number of casing displacements. We conclude that the axial movement of the casing does not have a major impact on the hydraulic aperture of the microannulus. Shear displacement can increase the fracture permeability (typically in the direction perpendicular to the displacement), if it is accompanied by dilation normal to the fracture face⁴⁶. However, the particular geometry and boundary conditions in a wellbore do not allow for normal dilation at the casing-cement interface. In addition, the direction of flow is the same as the shear displacement which makes it less likely to alter the permeability. This explains the small impact of casing displacements on the permeability of the microannulus. The small increase or decrease in hydraulic aperture after each displacement can likely be attributed to changes in the surface roughness of the microannulus arising from the frictional forces between the casing and cement surfaces.

4.2. Residual aperture

The microannuli never fully closed in our tests, even though casing pressures reached values as high as 40 MPa. Based on Fig. 4, hydraulic apertures of the microannuli reach a relatively constant value at high casing pressures. This likely indicates that there is sufficient roughness between the surfaces of the casing and cement to allow for flow to exist even at high casing pressures. We define the residual aperture as the hydraulic aperture of the microannulus at high casing pressures, when the change in hydraulic aperture with casing pressure becomes negligible (within the range of pressures in this work). Fig. 7 visualizes the residual aperture of the microannulus for the CP-60-L and CP-7.5-L experiments.

Residual apertures in this work were observed to be dependent on the fluid pressure inside the microannulus (Table 3). Once the two faces of the microannulus come into contact, the roughness of the two surfaces will leave a flow path open. This

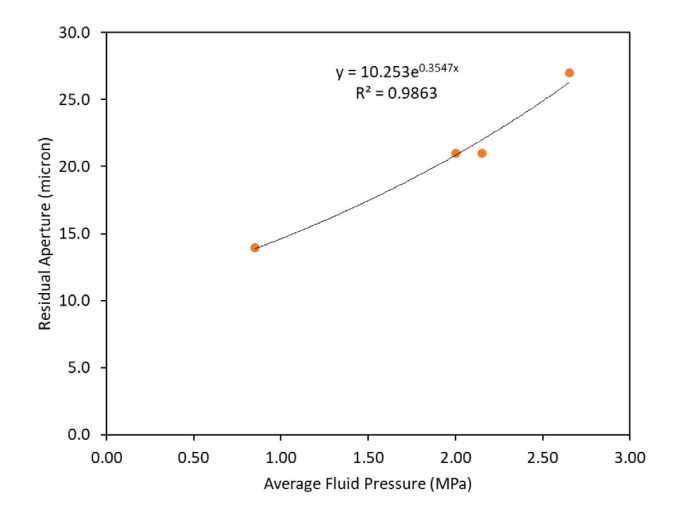


Fig. 8. Residual aperture versus average fluid pressure for the casing pressure tests

flow path could be envisioned as a compressible porous media. Therefore, the presence of pore pressure inside the microannulus could increase the residual aperture. The residual aperture's compressibility can then be defined as:

$$c_p = \frac{1}{e_r} \frac{\partial e_r}{\partial P} \tag{2}$$

Integrating Eq. (2), we obtain the following relationship between the residual aperture and fluid pressure:

$$e_r = e_i \exp(c_p P) \tag{3}$$

where, e_r is the residual aperture, e_i is the intrinsic residual aperture (at zero fluid pressure), c_p is compressibility, and P is the fluid pressure in the microannulus. Fig. 8 shows the relationship between the residual aperture and the average fluid pressure for the casing pressure tests (Fig. 4). According to Fig. 8, the intrinsic residual aperture and the compressibility of the microannulus for the first sample are approximately 10 μ m, and 0.35 MPa⁻¹, respectively.

The presence of a residual aperture is also supported by other annular flow experiments reported in the literature. 28,31 Thermally generated microannuli in the study by Stormont et al. 31 indicated a residual aperture of approximately 5 μm . The experiments reported by Boukhelifa et al. 28 showed residual apertures within 5 to 10 μm . Both these studies were conducted at low fluid pressures. Therefore, the reported values are indicative of intrinsic residual apertures. The large-scale experiments in this work show an intrinsic residual value of 10 μm which is on the higher end of the small-scale experiments by Stormont et al. 31 and Boukhelifa et al. 28

The intrinsic residual aperture could be correlated with the surface roughness of the cement at the casing–cement interface. 35,47 Welch et al. 32 conducted shear tests using a triaxial direct shear apparatus. The samples were cylindrical (2.5 × 2.5 cm), split vertically with half comprised of cement and the other half of steel. They performed surface profilometry of the cement surfaces after the shear tests and reported a mean-squared roughness of 10.8 and 4.8 μm depending on the curing time. The reported hydraulic apertures were in the same order of magnitude. The surface roughness values measured by Welch et al. 32 are close to the intrinsic residual aperture in this work. It should be noted that their measurements were conducted after shearing tests which could have impacted the surface roughness of the cement. The scale and the geometry of the cement surfaces

in this work are also very different than the samples used by Welch et al.³², which could lead to different roughness values. Existence of a residual aperture at the microannuli has important consequences for well leakage. The residual aperture could maintain a minimum level of fluid leakage that cannot be mitigated by means of mechanical loading. However, it can be mitigated by chemical processes such as precipitation of minerals.⁴⁸ Further investigations on the relationship between the residual aperture of the microannuli and surface roughness is needed to identify optimum leakage mitigation measures.

4.3. Hydraulic versus mechanical apertures

In this work, we used a finite element model to calculate the mechanical aperture of the microannulus at the casing–cement interface. However, the aperture values calculated from the flow experiments represented the hydraulic apertures of the microannuli. Hydraulic aperture is usually smaller than the mechanical aperture due to roughness of the microannulus surface and flow path tortuosity. They can be assumed to be equal when the roughness between the two surfaces is much smaller than the aperture size. The roughness of the cement surface is likely of the same order of magnitude as the aperture sizes in our experiments. Therefore, we expect a difference between the magnitude of the mechanical and hydraulic apertures.

Geomechanical modelling is an effective way to assess the integrity of the annular cement in the wellbores under different geological and operational settings.²² These models have been also used to predict the aperture of the microannulus considering the operational history of a well.^{18,37} However, the model predictions are mechanical apertures which need to be translated to hydraulic apertures to estimate well leakage. To bridge the gap between the model predictions and annular fluid leakage, we need to understand the relationship between the mechanical and hydraulic apertures of the microannulus.

The relationship between the hydraulic and mechanical apertures of fractures has been extensively studied.^{38–41} Barton et al.⁴⁰ proposed the following empirical relationship between the hydraulic and the mechanical aperture and the Joint Roughness Coefficient (JRC):

$$e_h = \frac{e_m^2}{IRC^{2.5}} \tag{4}$$

where, e_h is the hydraulic aperture, e_m is the mean mechanical aperture and JRC is the joint roughness coefficient as defined by Barton and Choubey⁵⁰. More sophisticated correlations have been proposed that incorporate the standard deviation of the mechanical aperture measurements, and contact area between the two faces of the fractures.^{39,41,51,52} An important shortcoming of Eq. (4) and other correlations in the literature is that they do not result in a residual hydraulic aperture when the mechanical aperture approaches zero. We propose the following relationship that honors the observation of residual aperture in the experiments:

$$\frac{e_h}{e_r} = \exp(a\frac{e_m}{e_r}) \tag{5}$$

where, e_r is the residual hydraulic aperture, e_h and e_m are the hydraulic and mean mechanical apertures, and a is an empirical parameter. In Eq. (5), mechanical and hydraulic apertures are normalized using the residual aperture. For elastic deformation of asperities, we can replace the expression for the residual aperture from Eq. (3) in Eq. (5) to obtain:

$$\frac{e_h}{e_i \exp(c_p P)} = \exp(a \frac{e_m}{e_i \exp(c_p P)})$$
 (6)

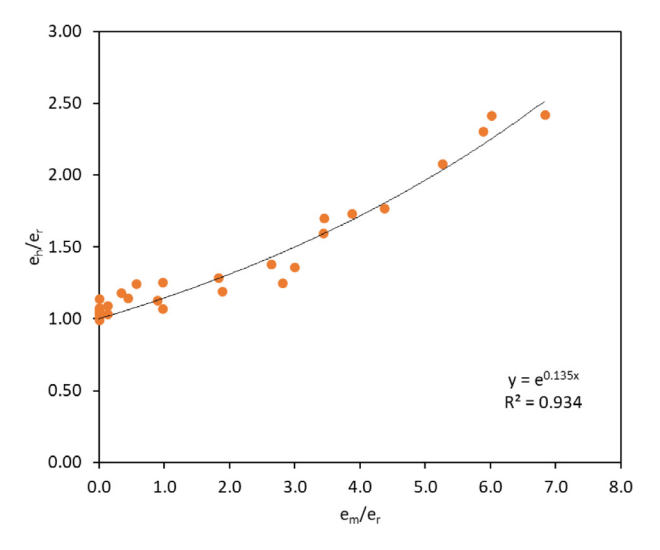


Fig. 9. Plot of the normalized hydraulic apertures from the casing pressure experiments versus the normalized mechanical apertures from the numerical modelling results.

Based on Eq. (6), as the mechanical aperture approaches zero, hydraulic aperture approaches the residual value (which is dependent on flowing fluid pressure), as observed in our experimental results. Both the intrinsic residual aperture and the parameter a are expected to be related to the roughness of the cement surface. Using an intrinsic residual aperture of 10 μ m, and a compressibility of 0.35 MPa $^{-1}$ (obtained from Fig. 8), Fig. 9 presents a plot of the normalized hydraulic apertures from our casing pressure experiments and the normalized mechanical apertures from the numerical results.

A curve fit of the data presented in Fig. 9 returns a value of 0.135 for parameter a with a R^2 of 0.934. Using this value for a, Fig. 10 provides a plot of the hydraulic versus mechanical apertures calculated using Eq. (6), assuming an intrinsic residual aperture of 10 µm. The hydraulic apertures measured in this work are also plotted against the mechanical apertures estimated using the numerical model. Fig. 10 indicates that Eq. (6) can describe the relationship between the mechanical and hydraulic apertures with reasonable accuracy. Average fluid pressures of 0.5 and 2.5 MPa are considered in Fig. 11, as they represent the lower and upper bounds of fluid pressure in the experiments. According to Fig. 10, due to the presence of a residual hydraulic aperture, e_h is higher than e_m at low mechanical apertures. However, as the mechanical aperture increases, it eventually exceeds the hydraulic aperture. Barton's (1985) equation (Eq. (4)) is also plotted in Fig. 10, assuming a IRC of 6 to best fit the experimental data. The results show that Eq. (4) does not adequately describe the trend in the experimental results.

In order to use Eq. (6), an estimate of the intrinsic residual aperture is required. This could be dependent on surface roughness of the cement at the microannulus interface. The results of our large-scale experiments indicate an intrinsic residual aperture of 10 μ m and residual aperture values ranging between 15 and 30 μ m, depending on the fluid pressure. Based on this range of residual apertures, our results show that setting the fitting constant "a" equal to 0.135, sufficiently describes the data. It must be noted that if the residual aperture magnitude changes significantly, the value of a should also be scaled accordingly. In addition, at high mechanical apertures (over 1000 μ m in the present case), Eq. (6) returns e_h values higher than e_m , which would be incorrect. At high mechanical apertures, hydraulic and mechanical apertures are equal. Therefore, Eq. (6) should only

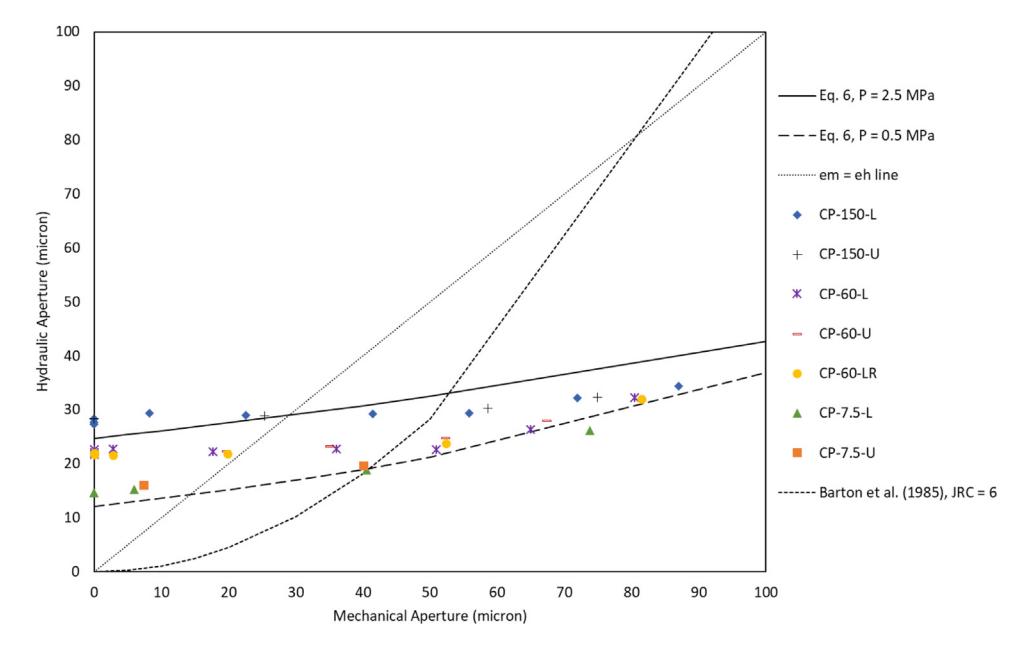


Fig. 10. Plot of the hydraulic versus mechanical apertures using Eq. (4) and Eq. (6) at fluid pressures of 0.5 and 2.5 MPa, along with the experimental results.

be used for the lower range of mechanical apertures, ideally below 500 μ m. This range should be sufficient for well integrity problems including a microannulus. The same restriction applies to classic relationships between e_h and e_m , such as in Eq. (4).

Eq. (6) provides a new relationship between the mechanical apertures calculated using well integrity models and the hydraulic apertures that determine fluid leakage through microannuli. Using the mechanical aperture calculations to determine flow can greatly overestimate the fluid leakage along a wellbore if a microannulus is open. Subsequently, if the microannulus is formed but is closed due to high casing pressures or temperatures, fluid leakage could be underestimated by relying solely on the results of the mechanical models. Therefore, incorporating the results of this work in well leakage models will yield better forecasts of critical apertures for loss of zonal isolation and assessment of potential fluid leakage rates.

4.4. Implications for well leakage calculation

In order to assess the applicability of the measured hydraulic aperture values in this work to actual well leakage scenarios, we performed a literature review for methane emission measurements from oil and gas wells. There are several recent studies that have measured methane emissions at oil and gas wellheads (Table 4), using a static chamber methodology.⁵³ The measurements were calibrated by recording the baseline methane emissions in the vicinity of the wells. Table 4 summarizes the results of 10 leakage datasets. 8 of the datasets were gathered from the United States, 1 from the UK, and the remaining dataset was from abandoned oil and gas wells in the Netherlands. Each dataset contained several wells, ranging from 19 to 147. Each publication has reported different statistical parameters and different units of leakage. To make the comparison possible, we have only summarized the average and the maximum leakage rates encountered in their results, in kg/yr. The average leakage rates in these datasets are relatively small, ranging between 0 and 364 kg/yr for abandoned wells and 1218 kg/yr for active wells. To put these numbers into perspective, a dairy cow on average releases 100 kg of methane per year.⁵⁴ However, in most cases the maximum leak rate was at least an order of magnitude higher than the average. The max leakage rates in all datasets ranged between 2 and 3881 kg/yr for abandoned wells, and 28286 kg/yr for actively producing wells. It should be noted that only one dataset included measurements for active wells. More leakage measurements on active wells are needed to improve the confidence for this comparison.

We wish to investigate whether the magnitude of the leak rates observed in the field-scale measurements are in line with the hydraulic apertures measured in this work, *should* microannuli develop along the entire well sections from leak source to surface. To this end, we designed a thought experiment of a hypothetical abandoned well with a microannulus connecting a gas pocket to surface. The gas bearing formation was assumed to be 1500 metres deep at hydrostatic pore pressure. We calculated the hypothetical steady-state methane leakage to surface considering various aperture sizes using Eq. (7). Eq. (7) presents a more generalized form of Eq. (1), suitable for calculating gas leakage through a microannulus.⁶⁰

$$\dot{m} = \frac{\rho(P,T)}{\mu(P,T)} \times \frac{\pi Re_h^3}{6} \frac{\partial (P - \rho gz)}{\partial z}$$
 (7)

 \dot{m} is the mass flow rate of gas, ρ and μ are gas density and viscosity, R is the casing outer radius, e_h is the hydraulic aperture of the microannulus, P is the gas pressure, and z represents depth. Eq. (7) considers the impact of gravity, which is significant in case of gas leakage to surface. Other assumptions in Eq. (7) include steady-state flow, single phase fluid, and laminar flow regime. Gas density and viscosity are strong functions of pressure and temperature. This complexity hinders a straightforward solution to Eq. (7). We calculated the gas rate in Eq. (7) numerically, using a procedure similar to Hongjun et al. 61 . Peng and Robinson 62 equation of state was used for calculating methane compressibility (used for density calculations) and the measurements by Lee et al. 63 were used to estimate methane viscosity.

Fig. 11 provides a summary of the maximum and average leakage rates measured in all the datasets covered in this work. Additionally, the dashed horizontal lines in Fig. 11 illustrate the calculated leakage rates at specific hydraulic aperture sizes, using Eq. (7). The results show that the average leak rates reported in the datasets correspond to average hydraulic aperture sizes in the range of 1 to 30 μ m. The maximum measured leak rates correspond to average aperture sizes between 2 and 100 μ m. This

Table 4Summary of the leak rate measurements at the wellheads of oil and gas wells.

Source	Location	No. of wells	Status	Max leak rate (kg/yr)	Average leak rate (kg/yr)
55	Pennsylvania, US	19	Abandoned - plugged and unplugged	876	99
56	West Virginia, US	112	Abandoned - plugged	105	1
56	West Virginia, US	147	Abandoned - unplugged	1551	27
56	West Virginia, US	79	Active	28286	1218
57	US - 4 States	119	Abandoned - plugged	2	0
57	US - 4 States	19	Abandoned - unplugged	1276	88
58	Pennsylvania, US	53	Abandoned - unplugged	3066	193
58	Pennsylvania, US	35	Abandoned - plugged	2540	131
59	UK	102	Abandoned - plugged	1718	364
34	Netherlands	29	Abandoned - plugged	3881	135



Fig. 11. Average and max leak rate measurements from various datasets compared to the calculated leakage rates using Eq. (7) (shown as dashed lines).

is an overly simplistic well leakage scenario, as in reality leakage pathways are likely formed from a combination of microannuli, shear and radial cracks, cement channels, and uncemented segments. However, this analysis provides a first screening of the magnitude of the leakage rates that could be caused by the range of microannuli apertures measured in this work, and how they compare to actual field measurements at the wellhead. It is of interest to assess whether typical microannuli apertures from models and experiments and the associated leakage rates are in line with the leakage measurements in the field cases.

Fig. 12 demonstrates a contour plot of predicted surface leakage rates of methane considering a range of hydraulic aperture sizes and depths of the gas source, assuming hydrostatic pressures. Eq. (7) was used to generate this plot assuming that the microannulus connects the gas formation to the surface. This plot can be used to obtain a quick estimate of the expected leakage rate in a well, by estimating the mechanical aperture of the microannulus using geomechanical models and converting it to the hydraulic aperture using Eq. (6). Conversely, we can identify the maximum allowable hydraulic aperture size in a well to keep the leakage below a threshold. For instance, Fig. 12 indicates that

if hydraulic aperture can be maintained below 20 µm leakage rates are below $\sim 100 \text{ kg/yr}$ (equivalent to methane emissions of a dairy cow) regardless of the depth of the gas source. These aperture estimates are likely conservative as the presence of water in the microannuli further hampers gas migration. This range is close to the residual aperture values measured in this work. In other words, while the microannulus does not seem to fully close, keeping its hydraulic aperture at the residual value can limit the leakage rate to amounts that are negligible compared to natural baselines. Assessment of these critical thresholds can assist operators and regulators in designing well abandonment conditions based on geomechanical models of the near wellbore region. One role of well integrity analyses is to identify and mitigate the likelihood of significant leaks from wells. The combined large-scale laboratory measurements and geomechanical modelling approach in this study provides a methodology to forecast the hydraulic apertures that can be present in the subsurface. This methodology could therefore be used to assess the leakage risks for new and abandoned wells.

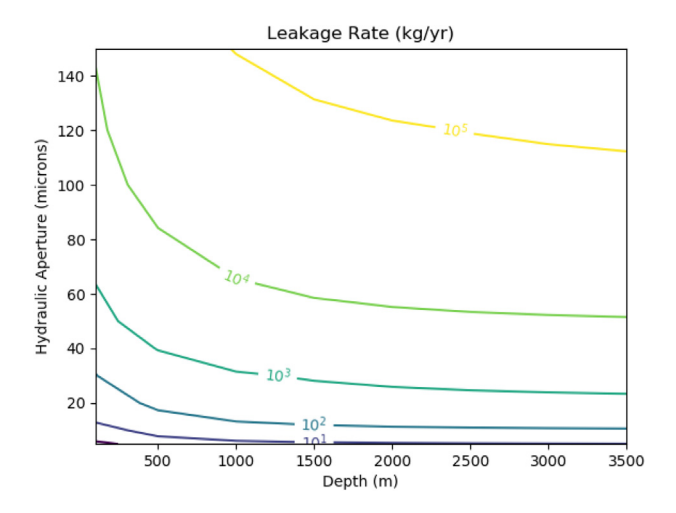


Fig. 12. Contour of surface leakage rates of methane at various source depths and aperture sizes assuming a hydrostatic pressure gradient.

5. Conclusions

In this study, we combined experimental analysis and numerical modelling to assess microannuli development and leakage rates at the casing-cement interface. We conducted a large-scale experimental campaign to understand the change in the hydraulic aperture of the microannuli at the casing-cement interface, under different loading conditions. The results provide valuable insights into the mechanisms of aperture development and sealing capacity of the cement sheath. The hydraulic aperture of the casing-cement microannuli in a large-scale setup was measured to be in the range of tens of microns. The hydraulic aperture decreased as the casing was pressurized to 40 MPa, but it remained open. A residual hydraulic aperture between 15 and 30 μm was observed in our results. Our results show that axial displacement of the casing does not significantly change the hydraulic aperture of the microannulus. A finite element numerical model was used to simulate the mechanical aperture of the microannuli under the same conditions as the experiments. We investigated the relationship between the mechanical and hydraulic apertures of the microannuli. A new equation is proposed to predict the hydraulic aperture of microannuli using the mechanical aperture determined by numerical simulations. The proposed equation captures the residual hydraulic aperture observed in our experimental results.

A review of field-scale measurements of methane leakage from abandoned wells support the order of magnitude of the hydraulic apertures determined in the present experiments and models. The large-scale laboratory measurements and modelling results in this work provide a methodology to use geomechanical models to forecast the hydraulic apertures that can be present in the subsurface. The methodology could be used by operators and regulators to determine the leakage risk of wells, and to devise effective leakage mitigation and well abandonment strategies.

CRediT authorship contribution statement

Al Moghadam: Conceptualization, Formal analysis, Writing – original draft, Visualization, Validation. **Koen Castelein:** Methodology, Investigation, Validation, Resources. **Jan ter Heege:** Conceptualization, Writing – review & editing. **Bogdan Orlic:** Formal analysis, Supervision, Writing – review & editing.

Declaration of competing interest

The authors declare that they have no known competing financial interests or personal relationships that could have appeared to influence the work reported in this paper.

Acknowledgements

This work was performed within the knowledge development project *Re-use and Decommissioning* sponsored by the Dutch government, The Netherlands. This work was also a part of the *SECURe* project funded by the European Union's Horizon 2020 research and innovation program under grant agreement number 764531. Large-scale experiments were conducted at the Rijswijk Centre for Sustainable Geoenergy (RCSG). We would like to thank Kaj Valk and Jens Wollenweber for their contribution to the project and Matteo Loizzo for the scientific review of the manuscript.

References

- Viswanathan HS, Pawar RJ, Stauffer PH, Kaszuba JP, et al. Development of a hybrid process and system model for the assessment of wellbore leakage at a geologic CO₂ sequestration site. *Environ Sci Technol*. 2008:42(19):7280–7286.
- Vidic RD, Brantley SL, Vandenbossche JM, Yoxtheimer D, Abad JD. Impact of shale gas development on regional water quality. Science. 2013;340(6134):1235009.
- 3. Bennett T. Well Cement Integrity and Cementing Practices. Report. Australia: University of Adelaide; 2016.
- Bois A-P, Garnier A, Galdiolo G, Laudet J-B. Use of a mechanistic model to forecast cement-sheath integrity. SPE Drill Completion. 2012;27(02):303-314.
- Zhang M, Bachu S. Review of integrity of existing wells in relation to CO₂ geological storage: what do we know? *Int J Greenh Gas Control*. 2011;5(4):826–840.
- Davies RJ, Almond S, Ward RS, Jackson RB, et al. Oil and gas wells and their integrity: Implications for shale and unconventional resource exploitation. *Mar Petrol Geol.* 2014;56:239–254.
- Kaldal GS, Jonsson MT, Palsson H, Karlsdottir SN. Structural modeling of the casings in high temperature geothermal wells. Geothermics. 2015;55:126–137.
- 8. Miyazaki B. Well integrity: An overlooked source of risk and liability for underground natural gas storage. Lessons learned from incidents in the USA. In: Evans DJ, Chadwick RA, eds. *Underground Gas Storage: Worldwide Experiences and Future Development in the UK and Europe. Vol. 313, No. 1.* Geological Society, London, Special Publications; 2009:163–172.
- Orlic B, Chitu A, Brunner L, Koenen M, Wollenweber J, Schreppers G-J. Numerical investigations of cement interface debonding for assessing well integrity risks. In *Proceedings of the 52nd US Rock Mechanics / Geomechanics* Symposium, ARMA 18-1298; 2018.
- Gill SK, Pyatina T, Sugama T. Thermal shock resistant cement. GRC Trans. 2012;36:445–452.
- Vrålstad T, Skorpa R, Werner B. Experimental studies on cement sheath integrity during pressure cycling. In: Paper SPE 194171 Presented at the SPE/IADC International Drilling Conference and Exhibition. The Hague, The Netherlands; 2019.
- Dusseault MB, Bruno MS, Barrera J. Casing shear: Causes, cases, cures. SPE Drill Completion. 2001;9:8–107.
- Bois A-P, Garnier A, Rodot F, Sain-Marc J, Aimard N. How to prevent loss of zonal isolation through a comprehensive analysis of microannulus formation. SPE Drill Completion. 2011;26(01):13–31.
- Lavrov A, Torsæter M, Albawi A, Todorovic J, Opedal N, Cerasi P. Near-Well integrity and thermal effects: a computational road from laboratory to field scale. In: Proceedings of the 48th US Rock Mechanics / Geomechanics Symposium, ARMA 14-7109; 2014.
- TerHeege JH, Orlic B, Wollenweber J. Discrete element modelling of wellbore integrity in high temperature geothermal reservoirs. In: Proceedings of the 51st US Rock Mechanics / Geomechanics Symposium, ARMA 17-176; 2017.
- **16.** Gasda SE, Bachu S, Celia MA. Spatial characterization of the location of potentially leaky wells penetrating a deep saline aquifer in a mature sedimentary basin. *Environ Geol.* 2004;46:707–720.
- Roy P, Morris JP, Walsh SDC, Iyer J, Carroll S. Effect of thermal stress on wellbore integrity during CO₂ injection. Int J Greenh Gas Control. 2018;77:14–26.

- 18. Chu W, Shen J, Yang Y, Li Y, Gao D. Calculation of micro-annulus size in casing-cement sheath-formation system under continuous internal casing pressure change. *Petrol Explor Dev+*. 2015;42(3):414–421.
- Lecampion B, Quesada D, Loizzo M, Bunger A, et al. Interface debonding as a controlling mechanism for loss of well integrity: Importance for CO₂ injector wells. *Energy Procedia*. 2011;4:5219–5226.
- Thiercelin MJ, Dargaud B, Baret JF, Rodriquez WJ. Cement design based on cement mechanical response. SPE Drill Completion. 1998;13(04):266–273.
- 21. Bosma M, Ravi K, van Driel W, Schreppers GJ. Design approach to sealant selection for the life of the well. In: *Paper SPE 56536 Presented At the SPE Annual Technical Conference and Exhibition*. Houston, Texas; 1999.
- 22. Gray KE, Podnos E, Becker E. Finite-element studies of near-wellbore region during cementing operations: Part I. SPE Drill Completion. 2009;24(01):127–136.
- Lavrov A. Stiff cement, soft cement: Nonlinearity, arching effect, hysteresis, and irreversibility in CO₂-well integrity and near-well geomechanics. Int J Greenh Gas Control. 2018;70:236–242.
- 24. Frash LP, Carey JW. Engineering prediction of axial wellbore shear failure caused by reservoir uplift and subsidence. SPE J. 2018;23(04):1039–1066.
- Zhang W, Eckert A. Micro-annulus generation under downhole conditions: Insights from three-dimensional staged finite element analysis of cement hardening and wellbore operations. J Rock Mech Geotech Eng. 2020;12(6):1185–1200.
- Goodwin KJ, Crook RJ. Cement sheath stress failure. SPE Drill Completion. 1992;7(04):291–296.
- 27. Jackson PB, Murphey CE. Effect of casing pressure on gas flow through a sheath of set cement. *Paper SPE 25698 Presented at the SPE/IADC Drilling Conference*. Amsterdam, Netherlands; 1993.
- Boukhelifa L, Moroni N, James S, Le Roy-Delage S, Thiercelin MJ, Lemaire G. Evaluation of cement systems for oil and gas well zonal isolation in a full-scale annular geometry. SPE Drill Completion. 2005;20(1):44–53.
- Therond E, Bois A-P, Whaley K, Murillo R. Large-scale testing and modeling for cement zonal isolation in water-injection wells. SPE Drill Completion. 2017;32(04):290–300.
- **30.** De Andrade J, Sangesland S, Skorpa R, Todorovic J, Vrålstad T. Experimental laboratory setup for visualization and quantification of cement-sheath integrity. *SPE Drill Completion*. 2016;31(04):317–326.
- Stormont JC, Fernandez SG, Taha MR, Matteo EN. Gas flow through casingcement microannuli under varying stress conditions. Geomech Energy Env. 2018;1:1–13.
- Welch NJ, Frash LP, Harp DH, Carey JW. Shear strength and permeability of the cement-casing interface. Int J Greenh Gas Control. 2020;95:102977.
- **33.** Nowamooz A, Lemieux JM, Molson J, Therrien R. Numerical investigation of methane and formation fluid leakage along the casing of a decommissioned shale gas well. *Water Resour Res.* 2015;51:4592–4622.
- **34.** Schout G, Griffioen J, Hassanizadeh SM, de Lichtbuer GC, Hartog N. Occurrence and fate of methane leakage from cut and buried abandoned gas wells in the Netherlands. *Sci Total Environ*. 2019;659:773–782.
- **35.** Witherspoon PA, Wang JSY, Iwai K, Gale JE. Validity of cubic law for fluid flow in a deformable rock fracture. *Water Resour Res.* 1980:16(6):1016–1024.
- 36. Oil & Gas UK. Guidelines on Qualification of Materials for the AbandOnment of Wells. Issue 2. 2015.
- 37. Orlic B, Moghadam A, Brunner L, van Unen M, et al. A Probabilistic well integrity analysis workflow for leakage risk assessment: Case studies for shale gas and re-use for CCS. In: Proceedings of the 15th Greenhouse Gas Control Technologies Conference 2020.UAE; 2021.
- Olsson R, Barton N. An improved model for hydro-mechanical coupling during shearing of rock joints. Int J. Rock Mech Min. 2001;38:317–329.
- Barton N, Quadros EF. Joint aperture and roughness in the prediction of flow and groutability of rock masses. Int J Rock Mech Min Sci. 1997;34(3-4):252. e1-252.e14.

- Barton N, Bandis S, Bakhtar K. Strength, deformation and conductivity coupling of rock joints. Int J Rock Mech Min Sci Abstr. 1985;22:121–140.
- Choi S, Jeon B, Lee S, Jeon S. Experimental study on hydromechanical behavior of an artificial rock joint with controlled roughness. Sustainability. 2019:11(1014).
- API RP 10B- 2. Recommended Practice for Testing Well Cements. 2nd ed. American Petroleum Institute; 2013.
- Moghadam A, Castelein K, ter ter Heege J, van der Valk K, Orlic B, Wollenweber J. Large-scale laboratory investigation of the microannulus behavior in the casing-cement interface. In: Proceedings of the 54th US Rock Mechanics / Geomechanics Symposium, ARMA 20-1325; 2020.
- ABAQUS/Standard User's Manual, Version 619. Providence, RI: Dassault Systèmes Simulia Corp; 2019.
- 45. James SG, Boukhelifa L. Zonal isolation modeling and measurements past myths and today's realities. SPE Drill Completion. 2008;23:68-75.
- Chen Z, Narayan SP, Yang Z, Rahman SS. An experimental investigation of hydraulic behaviour of fractures and joints in granitic rock. *Int J. Rock Mech Min Sci.* 2000;37(7):1061–1071.
- **47.** Renshaw CE. On the relationship between mechanical and hydraulic apertures in rough-walled fractures. *J Geophys Res-Sol Ea.* 1995;100(12):24629–24636.
- Wolterbeek TKT, Ruckert F, van Moorsel SG, Cornelissen EK. Reactive transport and permeability evolution in wellbore defects exposed to periodic pulses of CO2-rich water. Int J Greenhouse Gas Control. 2019;91:102835.
- **49.** Iwai K. Fundamental Studies of Fluid Flow Through a Single Fracture [Ph.D. thesis]. Berkeley: University of California; 1976.
- Barton N, Choubey V. The shear strength of rock joints in theory and practice. Rock Mech. 1977;10(1–2):1–54.
- Matsuki K, Chida Y, Sakaguchi K, Glover P. Size effect on aperture and permeability of a fracture as estimated in large synthetic fractures. Int J Rock Mech Min Sci. 2006;43:726–755.
- 52. Zimmerman R, Bodvarsson G. Hydraulic conductivity of rock fractures. *Transp Porous Media.* 1996;23:1–30.
- Livingston GP, Hutchinson GL. Enclosure-based measurement of trace gas exchange: Applications and sources of error. In: Matson PA, Harris RC, eds. Biogenic Trace Gases: Measuring Emissions from Soil and Water. Oxford, UK: Blackwell Science; 1995:14–51.
- AEA. Options To Reduce Methane Emissions. Final Report: aEAT-3773 Prepared for DGXI: 1999.
- Kang M, Kanno CM, Reid MC, Zhang X, et al. Direct measurements of methane emissions from abandoned oil and gas wells. Proc Natl Acad Sci USA. 2014;111(51):18173–18177.
- Riddick SN, Mauzerall DL, Celia MA, Kang M, et al. Measuring methane emissions from abandoned and active oil and gas wells in West Virginia. Sci Total Env. 2019;651:1849–1856.
- Townsend-Small A, Ferrara TW, Lyon DR, Fries AE, Lamb BK. Emissions of coalbed and natural gas methane from abandoned oil and gas wells in the United States. Geophys Res Lett. 2016;43:2283–2290.
- Kang M, Christian S, Celia MA, Mauzerall DL, et al. Identification and characterization of high methane-emitting abandoned oil and gas wells. Proc Natl Acad Sci USA. 2016:113(48):13636–13641.
- Boothroyd IM, Almond S, Qassim SM, Worrall F, Davies RJ. Fugitive emissions of methane from abandoned, decommissioned oil and gas wells. Sci Total Env. 2016;547:461–469.
- Dake LP. Fundamentals of Reservoir Engineering. Vol. 8. 1st ed Elsevier Science; 1983.
- **61.** Hongjun Z, Yuanhua L, Dezhi Z, Deping Z, Feng W. Calculation analysis of sustained casing pressure in gas wells. *Pet Sci.* 2012;9:66–74.
- 62. Peng DY, Robinson DB. A new two-constant equation of state. *Ind Eng Chem Fundam.* 1976;15(1):59–64.
- 63. Lee AL, Gonzalez MH, Eakin BE. The viscosity of natural gases. *J Petrol Technol.* 1966;18(08):997–1000.